

Z_b tetraquark channel from lattice QCD and Born-Oppenheimer approximation

S. Prelovsek,^{1,2,3,*} H. Bahtiyar,^{2,4} and J. Petković^{1,2}

¹*Faculty of Mathematics and Physics, University of Ljubljana, Ljubljana, Slovenia*

²*Jozef Stefan Institute, Ljubljana, Slovenia*

³*Institute for Theoretical Physics, University of Regensburg, Regensburg, Germany*

⁴*Department of Physics, Mimar Sinan Fine Arts University, Bomonti 34380, Istanbul, Turkey*

Two Z_b hadrons with exotic quark structure $\bar{b}b\bar{d}u$ were discovered by Belle experiment. We present a lattice QCD study of the $\bar{b}b\bar{d}u$ system in the approximation of static b quarks, where the total spin of heavy quarks is fixed to one. The energies of eigenstates are determined as a function of the separation r between b and \bar{b} . The lower eigenstates are related to a bottomonium and a pion. The eigenstate dominated by $B\bar{B}^*$ has energy significantly below $m_B + m_{B^*}$, which points to a sizable attraction for small r . The attractive potential $V(r)$ between B and \bar{B}^* is extracted assuming that this eigenstate is related exclusively to $B\bar{B}^*$. The Schrödinger equation for $B\bar{B}^*$ within the extracted potential leads to one bound state below $B\bar{B}^*$ threshold, whose mass depends on the parametrization of the lattice potential. For certain parametrizations, the bound state is very close to the $B\bar{B}^*$ threshold and renders a narrow peak in the $B\bar{B}^*$ rate above threshold - these features could be related to $Z_b(10610)$ in the experiment.

The Belle experiment discovered two Z_b^+ states with exotic quark content $\bar{b}b\bar{d}u$, $J^P = 1^+$ and $I = 1$ in 2011 [1, 2]. The lighter $Z_b(10610)$ lies slightly above $B\bar{B}^*$ threshold and the heavier $Z_b(10650)$ just above $B^*\bar{B}^*$. The observed decay modes are $\Upsilon(1S, 2S, 3S)\pi^+$, $h_b(1P, 2P)\pi^+$, $B\bar{B}^*$ and $B^*\bar{B}^*$ [1–3], where the $B\bar{B}^*$ and $B^*\bar{B}^*$ largely dominate $Z_b(10610)$ and $Z_b(10650)$ decays, respectively. Many phenomenological theoretical studies of these two states have been performed, for example [4–17], and the majority indicates that $B^{(*)}\bar{B}^*$ Fock component is important.

We explore this channel within the first-principle lattice QCD. The only preliminary lattice study of this channel has been reported in [18, 19] and is reviewed below. No other lattice results are available since this channel presents a severe challenge. Scattering matrix would have to be determined using the Lüscher method for at least 7 coupled two-meson channels listed in the previous paragraph. Poles of the scattering matrix would render possible Z_b states. Following this path seems too challenging at present. Furthermore, the original Lüscher approach for two-particle scattering is not valid above the three-particle threshold.

In the present study we consider the Born-Oppenheimer approximation [20], inspired by the study of this system in [18, 19]. It is applied in molecular physics since ions are much heavier than other degrees of freedom. It is valuable also for the Z_b system $\bar{b}b\bar{d}u$, where b and \bar{b} represent heavy degrees of freedom (h), while the light quarks and gluons are light degrees of freedom (l), see for example [21, 22]. The simplification comes from the fact that the heavy degrees of freedom have large mass and therefore small velocity and kinetic energy.

In the first step we treat b and \bar{b} as static at fixed distance r (Figure 1a) and the main purpose is to determine eigen-energies $E_n(r)$ of this system. This energy

represents the total energy without the kinetic and rest energies of the b and \bar{b} , so $E_n(r)$ is related to the potential $V(r)$ felt by the heavy degrees of freedom. In the second step, we study the motion of the heavy degrees of freedom (with the physical masses) under the influence of the extracted potential $V(r)$. Solutions of the Schrödinger equation render information on possible (virtual) bound states Z_b , resonances and cross-sections.

The low-lying eigenstates of the system in Fig. 1a with quantum numbers (2) are related to two-hadron states in Figs. 1 (b-d)

$$B(0)\bar{B}^*(r), \quad \Upsilon(r)\pi(\vec{p}=0), \quad \Upsilon(r)\pi(\vec{p}\neq 0), \quad \Upsilon(r)b_1(\vec{0}). \quad (1)$$

The eigen-energy $E_n(r)$ related to $B\bar{B}^*$ in Fig. 1b is of major interest since Z_b lies near $B\bar{B}^*$ threshold [1]. The $\Upsilon(r)\pi(\vec{p})$ represent the ground state at small r . Here $\Upsilon(r)$ denotes the spin-one bottomonium where \bar{b} and b are separated by r . Pion can have zero or non-zero momentum $\vec{p} = \vec{n}\frac{2\pi}{L}$ since the total momenta of light degrees of freedom is not conserved in the presence of static quarks, i.e. pion momentum can change when it scatters on an infinitely heavy Υ . Our task is to extract energies of all these eigenstates $E_n(r)$ as a function of r . The only previous lattice study of this system [18] presents preliminary results based on Fock components $B\bar{B}^*$ and $\Upsilon\pi(0)$; the presence $\Upsilon\pi(\vec{p}\neq 0)$ was mentioned in [19], but not included in the simulation.

Quantum numbers and operators: We consider Z_b^0 that has quantum numbers $I=1$, $I_3=0$, $J^{PC}=1^{+-}$ and $J_z=0$ in experiment. The list of conserved quantum numbers is slightly different in the systems with two static particles. We study the system in Fig. 1a with quantum numbers

$$I = 1, \quad I_3 = 0, \quad \epsilon = -1, \quad C \cdot P = -1 \quad (2)$$

$$S^h = 1, \quad S_z^h = 0, \quad J_z^l = 0, \quad (h = \text{heavy}, \quad l = \text{light})$$

where the neutral system is considered where C -

conjugation can be applied (Fig. 1 shows the charged partner). Only the z-component of angular momenta for the light degrees of freedom (J_z^{light}) is conserved. The quantum number ϵ corresponds to the reflection over the yz plane. P refers to inversion with respect to mid-point between b and \bar{b} and C is charge conjugation, where only their product is conserved. The quantum numbers in (2) are conventionally denoted by Σ_u^- using the conventions from [23]¹.

The spin of the infinitely heavy quark can not flip via the interaction with gluons, so spin S^h of $\bar{b}b$ is conserved. We choose to study the system with $S^h = 1$, which can decay to Υ , while it can not decay to η_b and h_b since these carry $S^h = 0$. Note that the physical Z_b and $B\bar{B}^*$ with finite m_b can be a linear combination of $S^h = 1$ as well as $S^h = 0$, and we study only $S^h = 1$ component here. We have in mind this component, which includes $B\bar{B}^*$, $\bar{B}B^*$, \bar{B}^*B^* (O_1 in Eq. 3), when we refer to " $B\bar{B}^*$ " throughout this paper.

The eigen-energies E_n of the system in Fig. 1a are determined from the correlation functions $\langle O_i(t)O_j^\dagger(0) \rangle$. We employ 6 operators O_i that create/annihilate the system with quantum numbers (2) and resemble Fock components (1) in Figs. 1 (b-d)

$$\begin{aligned}
O_1 &= O^{B\bar{B}^*} \propto \sum_{a,b} \sum_{A,B,C,D} \Gamma_{BA} \tilde{\Gamma}_{CD} \bar{b}_C^a(0) q_A^a(0) \bar{q}_B^b(r) b_D^b(r) \\
&\propto ([\bar{b}(0)P_- \gamma_5 q(0)] [\bar{q}(r)\gamma_z P_+ b(r)] + \{\gamma_5 \leftrightarrow \gamma_z\}) \\
&\quad + ([\bar{b}(0)P_- \gamma_y q(0)] [\bar{q}(r)\gamma_x P_+ b(r)] - \{\gamma_y \leftrightarrow \gamma_x\}) \\
O_2 &= O^{B\bar{B}^*} \\
O_3 &= O^{\Upsilon\pi(0)} \propto [\bar{b}(0)U\gamma_z P_+ b(r)] [\bar{q}\gamma_5 q]_{\vec{p}=\vec{0}} \\
O_4 &= O^{\Upsilon\pi(1)} \propto [\bar{b}(0)U\gamma_z P_+ b(r)] ([\bar{q}\gamma_5 q]_{\vec{p}=\vec{e}_z} + [\bar{q}\gamma_5 q]_{\vec{p}=-\vec{e}_z}) \\
O_5 &= O^{\Upsilon\pi(2)} \propto [\bar{b}(0)U\gamma_z P_+ b(r)] ([\bar{q}\gamma_5 q]_{\vec{p}=2\vec{e}_z} + [\bar{q}\gamma_5 q]_{\vec{p}=-2\vec{e}_z}) \\
O_6 &= O^{\Upsilon b_1(0)} \propto [\bar{b}(0)U\gamma_z P_+ b(r)] [\bar{q}\gamma_x \gamma_y q]_{\vec{p}=\vec{0}}. \quad (3)
\end{aligned}$$

Here $\Gamma = P_- \gamma_5$, $\tilde{\Gamma} = \gamma_z P_+$, $[\bar{q}\Gamma'q]_{\vec{p}} \equiv \frac{1}{V} \sum_{\vec{x}} \bar{q}(\vec{x})\Gamma'q(\vec{x})e^{i\vec{p}\vec{x}}$, momenta is given in units of $2\pi/L$, capital (small) letters represent Dirac (color) indices, color singlets are denoted by $[\dots]$ and U is a product of gauge links between 0 and r . First line in O_1 decouples spin indices of light and heavy quarks in order to make J_z^l and $S_{(z)}^h$ (2) are more transparent [18], while the second line is obtained via the Fierz transformation. O_2 is obtained from O_1 by replacing all $q(x)$ with $\nabla^2 q(x)$. $O_{4,5}$ have pion momenta in z direction due to $J_z^l = 0$ and have two terms to ensure $C \cdot P = -1$. The Υb_1 is not a decay mode for finite m_b where C and P are separately conserved, but it has quantum numbers (2) for $m_b \rightarrow \infty$. The pair $\bar{q}q$ indicates

combination $\bar{u}u - \bar{d}d$ with $I = 1$ and $I_3 = 0$. All light quarks $q(x)$ are smeared around the position x using the full distillation [24] with the radius about 0.3 fm, while the heavy quarks are point-like.

We verified there are no other two-hadron states in addition to (1) with quantum numbers (2) and with non-interacting energies (4) below $m_B + m_{B^*} + 0.2$ GeV.

Lattice details: Simulation is performed on an ensemble with dynamical Wilson-clover u/d quarks, $m_\pi \simeq 266(5)$ MeV, $a \simeq 0.1239(13)$ fm and 280 configurations [25, 26]. We choose an ensemble with small $N_L = 16$ and $L \simeq 2$ fm so that $\Upsilon\pi(p_z)$ with $p_z > 2\frac{2\pi}{L}$ appear at $E > m_B + m_{B^*} + 0.2$ GeV above our interest; larger L would require further operators like $O_{4,5}$ with higher \vec{p} . Small L restricts us to $r/a \leq \frac{1}{2}N_L = 8$, but the statistical errors grow with r and the current precision prevents us from accurate results for $r/a > 8$ anyway. Small L leads also to the usual exponentially-suppressed corrections related to the pion and a very mild effect on the light-quark cloud in a B -meson since $r_B \ll L$. The lattice temporal extent $N_T = 32$ is effectively doubled by summing the light-quark propagators with periodic and anti-periodic boundary conditions in time [26].

Calculation of eigen-energies and overlaps: Correlation matrices $C_{ij}(t) = \langle O_i(t)O_j^\dagger(0) \rangle$ are evaluated using the full distillation method [24]. The $\bar{b}b$ annihilation Wick contraction is not present in the static limit considered here. C_{ij} are averaged over 8^3 or 16^3 space positions of \bar{b} , while sub-matrix for O_{3-6} is averaged over all source time slices to increase accuracy. Eigen-energies E_n and overlaps $\langle O_i|n \rangle$ are extracted from the 6×6 matrices $C_{ij}(t) = \sum_n \langle O_i|n \rangle e^{-E_n t} \langle n|O_j^\dagger \rangle$ using the widely used GEVP variational approach [27–29].

Eigen-energies of $\bar{b}b\bar{d}u$ system as a function of r : The main result of our study are the eigen-energies of the $\bar{b}b\bar{d}u$ system (Fig. 1a) with static b and \bar{b} separated by r . They are shown by points in Figure 2. The colors of points indicate which Fock-component (1) dominates an eigenstate, as determined from the normalized overlaps of an eigenstate $|n\rangle$ to operators O_i . Normalized overlap $\tilde{Z}_i^n \equiv \langle O_i|n \rangle / \max_m \langle O_i|m \rangle$ is normalized so that its maximal value for given O_i across all eigenstates is equal to one.

The dashed lines in Fig. 2 provide the related non-interacting (n.i.) energies E_n of two-hadron states (1)

$$E_{B\bar{B}^*}^{n.i.} = 2m_B, \quad E_{\Upsilon\pi(\vec{p})}^{n.i.} = V_{bb}(r) + E_\pi(\vec{p}), \quad E_{\Upsilon b_1(0)}^{n.i.} = V_{bb}(r) + m_{b_1}, \quad (4)$$

where $\bar{b}b$ static potential $V_{bb}(r)$, $E_\pi(\vec{p}) \simeq \sqrt{m_\pi^2 + \vec{p}^2}$, m_{b_1} and $m_B = m_{B^*} = 0.5224(14)$ (mass of $B^{(*)}$ for $m_b \rightarrow \infty$ without b rest mass) are determined on the same lattice.

The eigenstate dominated by $B\bar{B}^*$ has an energy close to $m_B + m_{B^*}$ for $r > 0.5$ fm, but it has significantly lower energy for $r \simeq [0.1, 0.4]$ fm (red circles in Fig. 2). This indicates sizable strong attraction between B and

¹ This provides irreducible representation $(J_z^l)_{CP}^\epsilon = \Sigma_u^-$, where the notation here and in [23] is related by $J_z^l \rightarrow \Lambda$, $J_z^l = 0 \rightarrow \Sigma$, $CP \rightarrow \eta$, $CP = -1 \rightarrow u$.

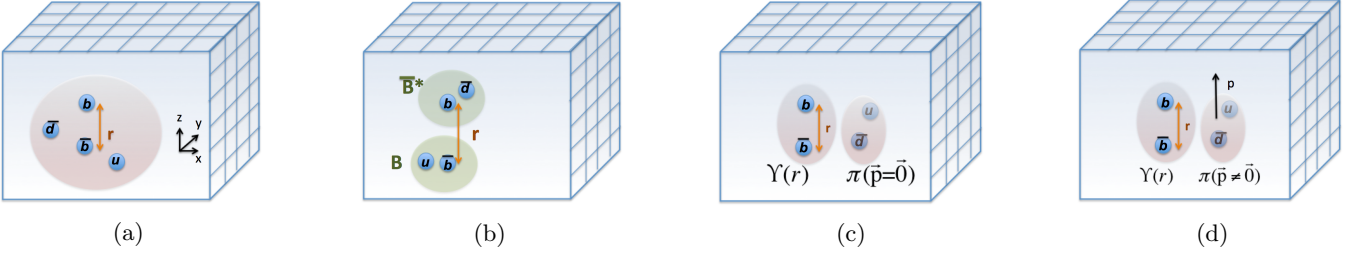


FIG. 1: (a) The system considered. (b-d) Two-hadron Fock components in the system with quantum numbers (2).

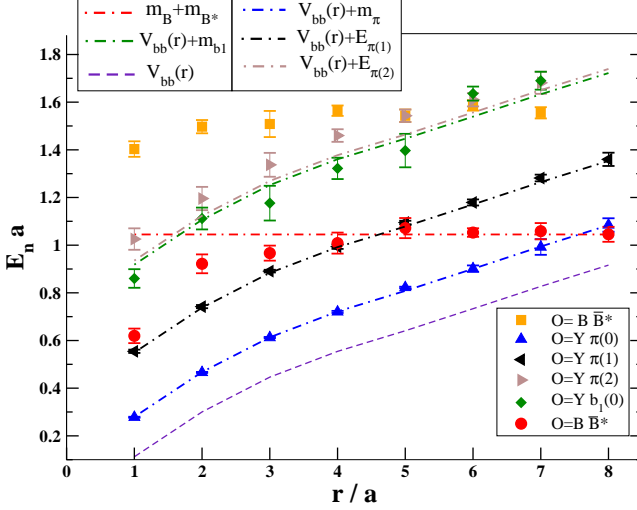


FIG. 2: Eigen-energies of $\bar{b}b\bar{u}$ system (Fig. 1a) for various separations r between static quarks b and \bar{b} are shown by points. The label indicates which two-hadron component dominates each eigenstate. The dot-dashed lines represent related two-hadron energies $E^{n.i.}$ (4) when two hadrons (1) do not interact. The eigenstate dominated by $B\bar{B}^*$ (red circles) has energy significantly below $m_B + m_{B^*}$ and shows sizable attraction. Lattice spacing is $a \simeq 0.124$ fm.

\bar{B}^* in this system - something that might be related to the existence of Z_b tetraquarks. This is the most important and robust result of this lattice study.

Other eigenstates are dominated by $\Upsilon\pi(\vec{p})$ and Υb_1 . Their energies E lie close to the non-interacting energies $E^{n.i.}$ (4) given by dot-dashed lines, so $E \simeq E^{n.i.}$. We point out that we can not claim nonzero energy shifts $E - E^{n.i.}$ for $\Upsilon\pi$ and Υb_1 states (although Fig. 2 shows small deviations from zero in some cases) since the statistical and systematic errors are not small enough.

Towards masses of Z_b states within certain approximations: Eigen-energies of $\bar{b}b\bar{u}$ system in Fig. 1a indicate that eigenstate dominated by the $B\bar{B}^*$ has significantly lower energy than $m_B + m_{B^*}$ at small separation r between static b and \bar{b} . This suggests a possible existence

of exotic hadron (related to Z_b) and related peak in the cross-section near $B\bar{B}^*$ threshold. Such physical observables require the study of the motion for the heavy degrees of freedom based on the energies $E_n(r)$ according to the Born-Oppenheimer approach. The precise prediction of such observables is not possible at present since lattice eigen-energies are not known for $r < a$. In addition, the accurate study would require the coupled-channel treatment of all Fock components (1) through the coupled-channel Schrödinger equation, which is a challenging task left for the future (this was recently elaborated in [30] for conventional $\bar{b}b$ with $I=0$).

We apply two simplifying approximations in order to shed light on the possible existence of Z_b based on energies in Figure 2. The first assumption is that the eigenstate indicated by red circles in Fig. 2 is related exclusively to $B\bar{B}^*$ Fock component and does not contain other Fock components in (1). This is supported by our lattice results to a very good approximation, since this eigenstate couples almost exclusively to $O^{B\bar{B}^*}$ and has much smaller coupling to $O^{\Upsilon\pi}$ and $O^{\Upsilon b_1}$: the normalized overlap of this state to $O^{\Upsilon\pi, \Upsilon b_1}$ is $\tilde{Z}_{3-6} \leq 0.07$ for $r/a \leq 3$, while overlap to $O^{B\bar{B}^*}$ is $\tilde{Z}_{1,2} \simeq \mathcal{O}(1)$. In the reminder we explore the physics implications of this eigen-energy $E_{B\bar{B}^*}(r)$.

The energy $E_{B\bar{B}^*}(r)$ represents the total energy without the kinetic energy of heavy degrees of freedom. The difference $V(r) = E_{B\bar{B}^*}(r) - m_B - m_{B^*}$ therefore represents the potential felt by the heavy degrees of freedom, in this case between B and \bar{B}^* mesons. The extracted potential is plotted in Fig. 3. The potential shows sizable attraction for $r = [0.1, 0.4]$ fm and is compatible with zero for $r \geq 0.6$ fm within sizable errors. Lattice study that would probe whether one-pion exchange dominates at large r would need higher accuracy.

The problem is that the potential $V(r)$ is not determined from the lattice for $r < a$, it might be affected by discretization effects at $r \simeq a$ and the analytic form of r -dependence is not known apriori. This brings us to the second simplifying approximation

$$V(r) = V_{reg.}(r) + V_{1/r}(r), \quad V_{reg.}(r) = -A e^{-(r/d)^F}, \quad (5)$$

where we assume a certain form of the regular potential $V_{reg.}(r)$ that has no singularity at $r \rightarrow 0$. The fits of

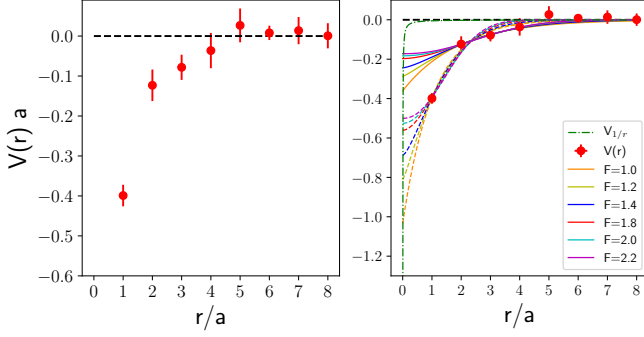


FIG. 3: (a) The extracted potential $V(r)$ between B and \bar{B}^* from lattice. (b) Fits of $V(r)$ assuming the form of the regular potential V_{reg} (5) are presented by the solid and dashed lines for various values of parameter F . Solid and dashed lines correspond to fits in the ranges $r/a = [2, 4]$ and $[1, 4]$, respectively. The singular potential $V_{1/r}(r)$ is shown by dot-dashed green line. Lattice spacing is $a \simeq 0.124$ fm.

the lattice potential for various choices of the parameter F (5) are shown in Fig. 3. We employ two choices of fitting ranges $r/a = [2, 4]$ or $[1, 4]$ since the lattice potential at $r/a = 1$ can be prone to the lattice discretization errors. The question if the potential contains also a singular piece $1/r$ can be addressed perturbatively, giving $V_{1/r}^{O(\alpha_s)}(r) = 0$ and $V_{1/r}(r) = \frac{1}{9}[V_0(r) + 8V_8(r)] = \frac{\delta a_2}{108\pi^2} \frac{\alpha_s^3}{r}$ [31] for very small r . This follows from the interaction of \bar{b} and b within $B\bar{B}^*$, while other pairs among $\bar{b}b\bar{q}q$ are at average distance of the order of B-meson size and do not lead to singularity at $r \rightarrow 0$. Results below are based on $V_{reg} + V_{1/r}$; we have verified that masses and cross-sections based solely on V_{reg} agree within the errors since $V_{1/r}$ is suppressed.

The motion of B and \bar{B}^* within the extracted potential $V(r)$ is analyzed by solving the non-relativistic 3D Schrödinger equation $[-\frac{1}{2\mu} \frac{d^2}{dr^2} + \frac{l(l+1)}{2\mu r^2} + V(r)]u(r) = Wu(r)$ for the experimentally measured $B^{(*)}$ meson masses and $1/\mu = 1/m_B^{exp} + 1/m_{B^*}^{exp}$. Here $W = E^{tot} - m_B - m_{B^*}$ is the energy with respect to $B\bar{B}^*$ threshold. The B and \bar{B}^* can couple to Z_b channel with $J^P = 1^+$ in partial waves $l = 0, 2$. Below we extract (virtual) bound states and scattering rates for $l = 0$, while $l = 2$ is not discussed since $V(r) + \frac{l(l+1)}{2\mu r^2} > 0$ is repulsive for all r .

The wave functions of the Schrödinger equation render the phase shift $\delta_{l=0}(W)$ and $B\bar{B}^*$ scattering matrix $S(W) = e^{2i\delta_0(W)}$. Resonances above threshold do not occur for purely attractive s-wave potentials since there is no barrier to keep the state metastable, while (virtual) bound states below threshold may be present. Bound state (virtual bound state) corresponds to the pole of $S(W)$ for real $W < 0$ and imaginary momenta $k = i|k|$

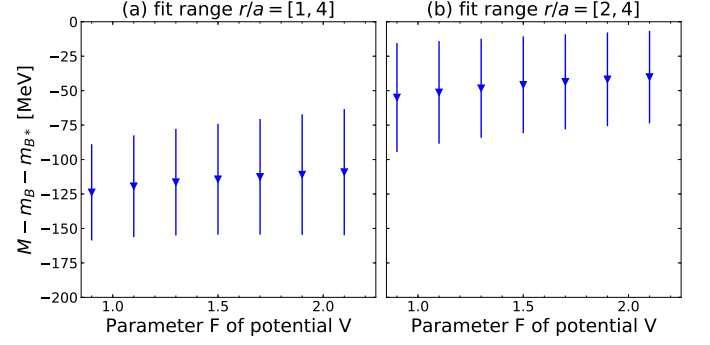


FIG. 4: The mass of the bound state for various fits of the potential $V(r)$. The mass is shown for various choices of the parameter F in $V(r)$ (5) and the fitting range in r .

($k = -i|k|$) of B in the center of momentum frame.

We find one bound state below threshold and its mass is shown in Fig. 4. The mass is presented for various choices of the parameter F in the potential (5) and the fitting ranges in r . The bound state with mass M lies at

$$M - m_B - m_{B^*} = -48^{+41}_{-108} \text{ MeV} . \quad (6)$$

The central value corresponds to fit of the potential (5) in the range $r/a = [2, 4]$ that renders the parameters $F = 1.3$, $A = 0.262(38)$, $d = 2.51(27)$. The significant uncertainty of the binding energy captures the statistical errors as well as various choices for parametrizing the potential in Fig. 4.

This bound state is responsible for a peak in the $B\bar{B}^*$ rate $N_{B\bar{B}^*} \propto k\sigma \propto \sin^2 \delta_0(W)/k$ above threshold if the bound state lies closely below threshold. This is illustrated in Fig. 5, which shows this rate for three fits that are all consistent with our lattice potential: the fit leading to the central value (6) and two choices of the fits that lead to a small or a large binding energy. The bound state with a small binding energy $\simeq 8$ MeV leads to a peak in the $B\bar{B}^*$ rate above threshold. Its shape resembles the $Z_b(10610)$ peak in the $B\bar{B}^*$ rate observed by Belle (Fig. 2 of [3]).

The significantly attractive $B\bar{B}^*$ potential (Fig. 3) and the resulting bound state in Fig. 4 could be related to the existence of Z_b in experiment. The reliable relation between both will be possible only when simplifications employed here will be overcome in the future simulations. The $Z_b(10610)$ was found as a virtual bound state slightly below threshold by the re-analysis of the experimental data [4] when the coupling to bottomonium light-meson channels was turned off [4] (the position of the pole is only slightly shifted when this small coupling is taken into account).

The exotic Z_b resonances were observed only by Belle, so their confirmation by another experiment would be

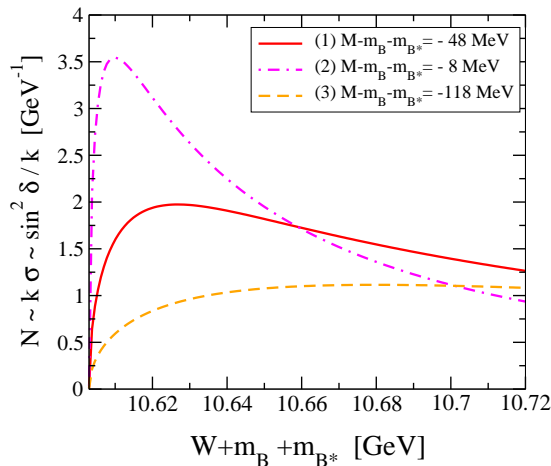


FIG. 5: The quantity $\sin^2 \delta / k$ that is proportional to the $B\bar{B}^*$ rate $N_{B\bar{B}^*} \propto k\sigma_{B\bar{B}^*}$. Three choices of fits consistent with our lattice potential are shown and the mass of the bound state is given for each case:

- (1) $F = 1.3, A = 0.26, d = 2.5$ (central value in Eq. 6),
- (2) $F = 2.0, A = 0.15, d = 2.8$ and
- (3) $F = 1.0, A = 1.0, d = 1.0$.

highly welcome. LHCb could try to search for it in inclusive final state $B\bar{B}^*$.

Comparison with a previous lattice study: Only one preliminary lattice study [18] of this channel was reported up to now, considering heavier $m_\pi = 480$ MeV and twisted-mass fermions. It employed operators $O^{B\bar{B}^*}$ and $O^{\Upsilon\pi(0)}$, while $O^{\Upsilon\pi(p \neq 0)}$ and $O^{\Upsilon b_1(0)}$ were omitted. Two eigenstates are interpreted as $\Upsilon\pi(0)$ and $B\bar{B}^*$. The resulting potential $V(r) = E_{B\bar{B}^*}(r) - m_B - m_{B^*}$ (red line in Fig. 1 of [18]) is also attractive and slightly weaker than our potential for small $r/a \simeq 1, 2$. This difference could be a consequence of a very different m_π . Their potential and its parametrization via $V(r) = -\frac{\alpha}{r}e^{-(r/d)^2}$ resulted in one bound state at $M - m_B - m_{B^*} = -58 \pm 71$ MeV in [18]. This is consistent with our binding energy shown in Fig. 4. Further lattice studies, including the comparison of the potentials at similar m_π , are highly awaited.

Conclusions: We presented a lattice QCD study of a channel with quark structure $\bar{b}b\bar{d}u$, where Belle observed two exotic Z_b hadrons. We find significantly attractive potential $V(r)$ between B and \bar{B}^* at small r when the total spin of the heavy quarks is equal to one. Dynamics of $B\bar{B}^*$ system within the extracted $V(r)$ leads to one bound state, whose mass depends on the parametrization of V . Certain parametrizations render a bound state closely below threshold and a narrow peak in $B\bar{B}^*$ rate just above threshold, resembling Z_b in experiment.

For quantitative comparison to experiment, future lattice studies need to explore how the dynamics of $B\bar{B}^*$ is influenced by the coupling to $\Upsilon\pi$ channels, and by the component where the total spin of the heavy quarks is

equal to zero. Derivation of the appropriate analytic form for $V(r)$ would be very valuable.

Acknowledgments

We thank G. Bali, V. Baru, P. Bicudo, N. Brambilla, E. Braaten, C. Hanhart, M. Karliner, R. Mizuk, A. Peters and M. Wagner for valuable discussions. S.P. acknowledges support by Research Agency ARRS (research core funding No. P1-0035 and No. J1-8137) and DFG grant No. SFB/TRR 55. H.B. acknowledges support from the Scientific and Technological Research Council of Turkey (TUBITAK) BIDEB-2219 Postdoctoral Research Programme.

Note added: In the previous version of this manuscript, the sub-matrix of the correlation matrix C_{ij} was multiplied by a wrong overall constant (that applied for the sub-matrix related to O_{3-6} that was averaged over source time slices). This affected the eigen-energies and overlaps. All figures (except for Fig. 1) are replaced and are based on the correct correlation matrices, while majority of text remains unmodified. The main conclusion does not change - Z_b is related to attraction between B and \bar{B}^* at small distance. The correct potential is less attractive and it results only in one bound state that is related to Z_b (the previous version quoted one virtual bound state slightly below threshold and an unexpected bound state far below threshold).

* sasa.prelovsek@ijs.si

- [1] Belle, A. Bondar *et al.*, Phys. Rev. Lett. **108**, 122001 (2012), [arXiv:1110.2251].
- [2] Belle, A. Garmash *et al.*, Phys. Rev. **D91**, 072003 (2015), [arXiv:1403.0992].
- [3] Belle, A. Garmash *et al.*, Phys. Rev. Lett. **116**, 212001 (2016), [arXiv:1512.07419].
- [4] Q. Wang *et al.*, Phys. Rev. **D98**, 074023 (2018), [arXiv:1805.07453].
- [5] X.-W. Kang, Z.-H. Guo and J. A. Oller, Phys. Rev. **D94**, 014012 (2016), [arXiv:1603.05546].
- [6] P. G. Ortega, J. Segovia, D. R. Entem and F. Fernández, The charged Z_c and Z_b structures in a constituent quark model approach, in *24th European Conference on Few-Body Problems in Physics (EFB24) Surrey, UK, September 2-6, 2019*, 2019, [1910.06579].
- [7] G.-J. Wang *et al.*, Eur. Phys. J. **C79**, 567 (2019), [arXiv:1811.10339].
- [8] Y.-C. Yang, Z.-Y. Tan, H.-S. Zong and J. Ping, Few Body Syst. **60**, 9 (2019), [arXiv:1712.09285].
- [9] M. B. Voloshin, Phys. Rev. **D96**, 094024 (2017), [arXiv:1707.00565].
- [10] F. Goerke, T. Gutsche, M. A. Ivanov, J. G. Körner and V. E. Lyubovitskij, Phys. Rev. **D96**, 054028 (2017), [arXiv:1707.00539].
- [11] J. M. Dias, F. Aceti and E. Oset, Phys. Rev. **D91**, 076001

- (2015), [arXiv:1410.1785].
- [12] F. K. Guo *et al.*, Phys. Rev. **D93**, 074031 (2016), [arXiv:1602.00940].
 - [13] A. Ali, C. Hambrock and W. Wang, Phys. Rev. **D85**, 054011 (2012), [arXiv:1110.1333].
 - [14] J. He, Phys. Rev. **D90**, 076008 (2014), [arXiv:1409.8506].
 - [15] M. Karliner and S. Nussinov, JHEP **07**, 153 (2013), [arXiv:1304.0345].
 - [16] M. Cleven *et al.*, Phys. Rev. **D87**, 074006 (2013), [arXiv:1301.6461].
 - [17] A. Esposito, A. Pilloni and A. D. Polosa, Phys. Lett. **B758**, 292 (2016), [arXiv:1603.07667].
 - [18] A. Peters, P. Bicudo, K. Cichy and M. Wagner, J. Phys. Conf. Ser. **742**, 012006 (2016), [arXiv:1602.07621].
 - [19] A. Peters, P. Bicudo and M. Wagner, EPJ Web Conf. **175**, 14018 (2018), [arXiv:1709.03306].
 - [20] M. Born and J. Oppenheimer, Ann. Physik **84**, 457 (1927).
 - [21] E. Braaten, C. Langmack and D. H. Smith, Phys. Rev. **D90**, 014044 (2014), [arXiv:1402.0438].
 - [22] N. Brambilla, G. Krein, J. Tarrus Castella and A. Vairo, Phys. Rev. **D97**, 016016 (2018), [arXiv:1707.09647].
 - [23] K.J. Juge, J. Kuti, C. Morningstar, Phys. Rev. Lett. **82**, 4400 (1999), [arXiv:9902336].
 - [24] Hadron Spectrum, M. Peardon *et al.*, Phys. Rev. **D80**, 054506 (2009), [arXiv:0905.2160].
 - [25] A. Hasenfratz, R. Hoffmann and S. Schaefer, Phys. Rev. **D78**, 054511 (2008), [arXiv:0806.4586].
 - [26] C. B. Lang, D. Mohler, S. Prelovsek and M. Vidmar, Phys. Rev. **D84**, 054503 (2011), [arXiv:1105.5636], [Erratum: Phys. Rev. D89, no.5, 059903(2014)].
 - [27] C. Michael, Nucl. Phys. **B259**, 58 (1985).
 - [28] M. Luscher and U. Wolff, Nucl. Phys. **B339**, 222 (1990).
 - [29] B. Blossier, M. Della Morte, G. von Hippel, T. Mendes and R. Sommer, JHEP **04**, 094 (2009), [arXiv:0902.1265].
 - [30] P. Bicudo, M. Cardoso, N. Cardoso and M. Wagner, 1910.04827.
 - [31] B. A. Kniehl, A. A. Penin, Y. Schroder, V. A. Smirnov and M. Steinhauser, Phys. Lett. **B607**, 96 (2005), [arXiv:hep-ph/0412083].

SUPPLEMENTARY INFORMATION

S1: SYMMETRIES AND OPERATORS

In this section we provide more details on the transformation properties of the investigated system in Fig. 1(a) with quantum numbers in Eq. (2). Transformations and quantum numbers are considered on the example of operators O_1 and O_4 (3). The first line in O_1 separates Dirac indices of the heavy and light quarks, which simplifies specific transformations.

The z-component of the angular momentum $J_z^l = 0$ is the eigenvalue related to the rotation of the light degrees of freedom around z-axes. The light-quark part of O_1 is $\bar{q}_B^b \Gamma_{BA} q_A^a \propto \bar{q}^b (1 - \gamma_t) \gamma_5 q^a$, which has angular momentum equal to zero indeed. The light degrees of freedom in O_4 are represented by the pion with momentum $\vec{p} \propto e_z$ and a straight gauge link path U between 0 and r. Both have z-component of the angular momentum equal to zero.

The quantum number $\epsilon = -1$ is related to the reflection of the light-degrees of freedom over yz plane, which is a product of rotation $R_{x,\pi}$ by π around x and inversion I with respect to the midpoint between 0 and r. The light-quark part $\bar{q}^b (1 - \gamma_t) \gamma_5 q^a$ of O_1 is invariant under rotations and has $P = -1$, therefore $\epsilon = -1$. The pion with momenta in z-direction within O_4 transforms as $\pi_{\vec{p}=\vec{e}_z} \xrightarrow{R_{x,\pi}} \pi_{-\vec{e}_z} \xrightarrow{I} -\pi_{\vec{e}_z}$, while the straight gauge link is invariant under this reflection, so $\epsilon = -1$.

The Dirac structure for the heavy quark part in all operators is $\bar{b}\gamma_z P_+ b$, which ensures $S^h = 1$ and $S_z^h = 0$.

The $C \cdot P = -1$ is related to the product of the charge-conjugation and inversion with respect to the mid-point between 0 and r. Both refer to the transformation of the light-degrees of freedom as well as the transformation of the static color sources². This is most conveniently accomplished by the usual transformation rules $\psi \xrightarrow{C} C\bar{\psi}^T$ and $\psi \xrightarrow{P} \gamma_t \psi$ for both $\psi = q$ and b , where this operation does not affect the heavy quark spin, while $C = i\gamma_2 \gamma_t$. The operator O_1 has $C \cdot P = -1$ since

$$\begin{aligned}
 O_1 &= \sum_{a,b} \bar{b}^a(0) \tilde{\Gamma} b^b(r) \bar{q}^b(r) \Gamma q^a(0) \\
 &\xrightarrow{C} \sum_{a,b} b^{aT}(0) C \tilde{\Gamma} C \bar{b}^{bT}(r) q^{bT}(r) C \Gamma C \bar{q}^{aT}(0) \\
 &= \sum_{a,b} \bar{b}^b(r) C \tilde{\Gamma}^T C b^a(0) \bar{q}^a(0) C \Gamma^T C q^b(r) \\
 &\xrightarrow{P} \sum_{a,b} \bar{b}^b(0) \gamma_t C \tilde{\Gamma}^T C \gamma_t b^a(r) \bar{q}^a(r) \gamma_t C \Gamma^T C \gamma_t q^b(0) = -O_1,
 \end{aligned} \tag{S1}$$

² If the color of the static source was not transformed under the charge-conjugation, the color-singlet $\bar{b}^a q^a \bar{q}^b b^b$ would transform under C -conjugation to $\bar{b}^a C \bar{q}^{aT} q^{bT} C b^b$, which is not gauge invariant.

where P exchanges positions 0 and r , $\gamma_t C \tilde{\Gamma}^T C \gamma_t = \tilde{\Gamma}$ for $\tilde{\Gamma} = \gamma_z P_+$, $\gamma_t C \Gamma^T C \gamma_t = -\Gamma$ for $\Gamma = P_- \gamma_5$, and dummy indices $a \leftrightarrow b$ can be exchanged in the last expression. The linear combination $\pi_{\vec{p}=\vec{e}_z} + \pi_{\vec{p}=-\vec{e}_z} \xrightarrow{C} \pi_{\vec{e}_z} + \pi_{-\vec{e}_z} \xrightarrow{P} -\pi_{-\vec{e}_z} - \pi_{\vec{e}_z}$ ensures good $C \cdot P = -1$ for O_4 .

The second line in operator O_1 (3) is obtained via the Fierz rearrangement

$$\tilde{\Gamma}_{CD} \Gamma_{BA} = \frac{1}{16} \sum_{\Gamma^1, \Gamma^2} \text{Tr}[\Gamma^1 \tilde{\Gamma} \Gamma^2 \Gamma] \Gamma_{CA}^1 \Gamma_{BD}^2 \quad (\text{S2})$$

and further simplifies since static heavy quarks appear in the combinations $P_+ b$ and $\bar{b} P_-$.

S2: EFFECTIVE ENERGIES AND OVERLAPS

Effective energies E_n^{eff} of the system in Fig. 1a are shown in Fig. S1(a) for separation $r/a = 2$ and all eigenstates $n = 1, \dots, 6$. They are obtained from the correlation matrices $C_{ij}(t)$ via variational approach $C(t)u_n(t) = \lambda_n(t)C(t_0)u_n(t)$, where the effective energies are given by the eigenvalues $E_n^{eff}(t) \equiv \ln[\lambda_n(t)/\lambda_n(t+1)]$. Reference time $t_0 = [2, 4]$ is used for various r and agreement in this range of t_0 is verified. Effective energies render eigen-energies E_n in the plateau region, indicated in the plots.

The overlaps $\langle O_i | n \rangle$ of each eigenstate n to employed operators O_i (3) are shown in terms of the normalized overlaps \tilde{Z}_i^n in Fig. S1(b). Here $\tilde{Z}_i^n \equiv \langle O_i | n \rangle / \max_m \langle O_i | m \rangle$ is normalized so that its maximal value for given O_i across all eigenstates is equal to one.

The effective energies (with fits) and overlaps of the eigenstate dominated by $B\bar{B}^*$ (red circles in Fig. 2) are presented in Fig. S2.

The previous paragraphs apply to the case when all six operators listed in (3) are employed. These operators interpolate all five two-hadrons states $B\bar{B}^*$, $\Upsilon\pi(\vec{p}=0, 1, 2)$, $\Upsilon b_1(\vec{p}=0)$ that are expected in the relevant energy region below $m_B + m_{B^*} + 0.2$ GeV. If one added further operators, for example replacing γ_5 by $\gamma_5 \gamma_t$ within $O^{\Upsilon\pi}$ or employing different smearing on the light quarks q , the resulting eigenvalues would reach plateau earlier in time. However it is expected that the resulting eigen-energies would be consistent with the ones obtained here; the exception could be the highest eigenstate indicated by yellow in Fig. 2 that is above our region of interest and is not employed in the interpretation of result here.

We investigated the eigen-energies and overlaps if some of the operators among (3) are omitted from the correlation matrix. Note that the results based on omitting any of $O^{\Upsilon\pi}$ or $O^{\Upsilon b_1}$ can not be regarded as reliable, since they lie below or near eigenstate $B\bar{B}^*$ of interest. We found, for example, that $\Upsilon\pi(2)$ eigenstate (denoted by

brown in Fig. 2) disappears from the spectrum if operator $O^{\Upsilon\pi(2)}$ is omitted. Similarly $\Upsilon\pi(0)$ eigenstate seem to disappear from the spectrum at intermediate t when $O^{\Upsilon\pi(0)}$ is omitted, but some of the effective energies show falling behavior at larger t , indicating a coupling to the lightest eigenstate $\Upsilon\pi(0)$. We note that all the results in this work are based on including all operators (3).

S3: POTENTIAL BETWEEN B AND \bar{B}^* FROM LATTICE

The lattice potential $V(r)$ between B and \bar{B}^* from Fig. 3a is tabulated in Table S1.

r/a	$V(r)a$
1	-0.399 ± 0.027
2	-0.123 ± 0.039
3	-0.078 ± 0.031
4	-0.036 ± 0.044

TABLE S1: Potential $V(r)$ between B and \bar{B}^* extracted from our simulation and plotted in Fig. 3a. Potential $V(r)$ for separations $r/a > 4$ is equal to zero within statistical and systematic errors.

S4: POTENTIAL BETWEEN B AND \bar{B}^* AT VERY SMALL SEPARATION r

Let us consider the potential between B and \bar{B}^* analytically, where b and \bar{b} are separated by a very small distance $r \ll r_B$, such that r is much smaller than average distance r_B between b and \bar{q} in $B^{(*)}$ meson (i.e. average radius r_B of a static $B^{(*)}$ meson). We address the question whether this potential has a singular form $V_{1/r}(r) = \frac{K}{r}$ for $r \rightarrow 0$ and determine prefactor K , while we omit all sub-leading contributions that are finite at $r \rightarrow 0$. Among all pairs of the four quarks $\bar{b}b\bar{q}q$, only the interaction between b and \bar{b} at very small r could give potential proportional to $1/r$. All other pairs are at average distance of the order of $O(r_B)$, which is finite for $r \rightarrow 0$; these pairs do not lead to infinite potential for $r \rightarrow 0$ and we therefore omit their contribution to $V_{1/r}$.

The task is therefore to determine potential between b and \bar{b} within a pair of color-singlet $B^{(*)}$ mesons

$$|B\bar{B}^*\rangle = \frac{1}{\sqrt{3}}(\bar{b}q)\frac{1}{\sqrt{3}}(\bar{q}b) = \frac{1}{3} \sum_{a=1,3} \sum_{b=1,3} \bar{b}_a q_a \bar{q}_b b_b. \quad (\text{S3})$$

The color structure with indices a and b matches with the employed operators $O^{B\bar{B}^*}$, while other indices will not be relevant below. In order to determine the potential, $|B\bar{B}^*\rangle$ is expressed in terms of color singlets and octets

$$|B\bar{B}^*\rangle = \frac{1}{3} \left\{ \left(\frac{1}{\sqrt{3}} \bar{b}b \right) \left(\frac{1}{\sqrt{3}} \bar{q}q \right) + \sum_{A=1, \dots, 8} \left(\frac{1}{\sqrt{2}} \bar{b} \lambda_A b \right) \left(\frac{1}{\sqrt{2}} \bar{q} \lambda_A q \right) \right\}.$$

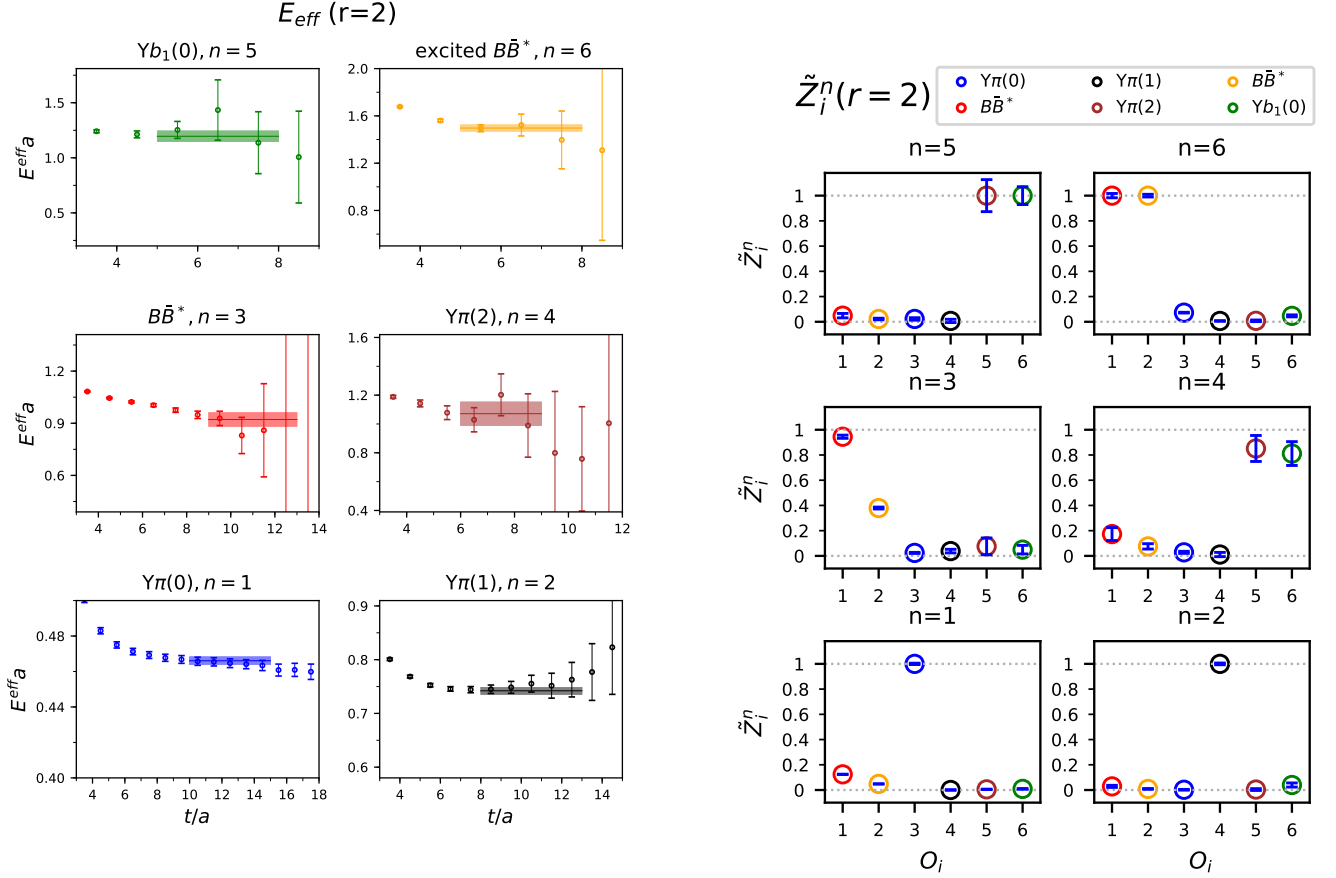


FIG. S1: (a) Effective energies E_n^{eff} of the system in Fig. 1a for separation $r/a = 2$ and all eigenstates $n = 1, \dots, 6$. They render eigen-energies E_n in the plateau region. (b) Normalized overlaps $\tilde{Z}_i^n \propto \langle O_i | n \rangle$ of each eigenstate n on the left to six operators $O_{i=1, \dots, 6}$. Absolute values of overlaps are shown for $r/a = 2$.

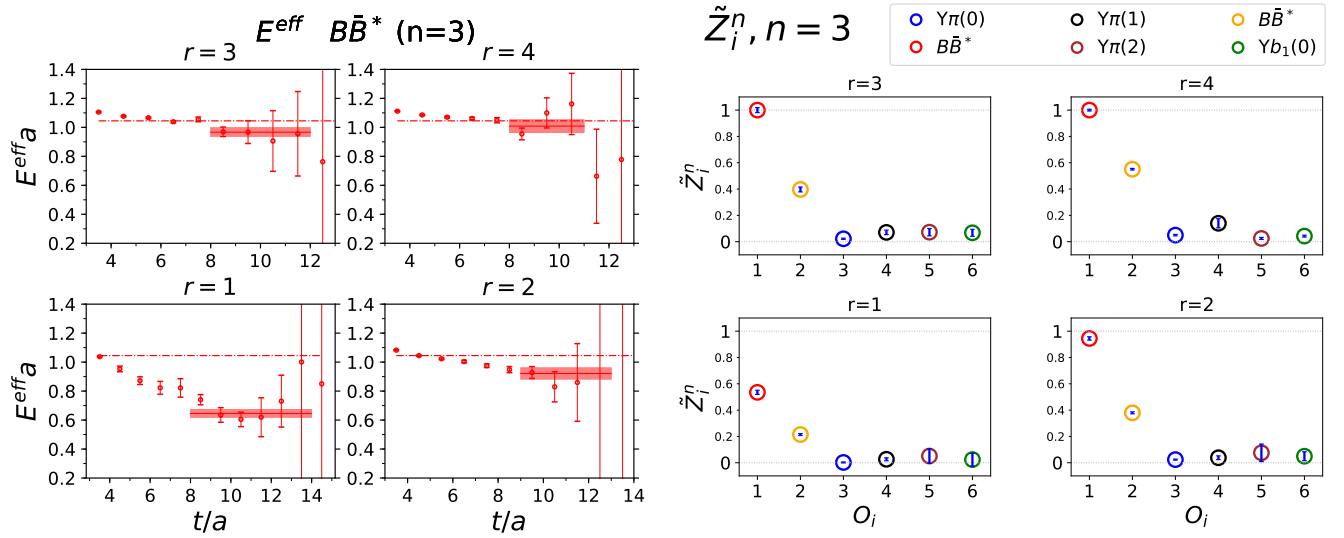


FIG. S2: Eigenstate dominated by $B\bar{B}^*$ (red circles in Fig. 2) for separations $r/a = [1, 4]$: (a) effective energies $E^{\text{eff}}(t)$ and (b) overlaps $\tilde{Z}_i^n \propto \langle O_i | n \rangle$, where the absolute value of the overlap is shown.

The $\bar{b}b$ singlet within $\langle B\bar{B}^* | B\bar{B}^* \rangle$ renders the singlet po-

tential $V_0(r)$, all eight octets render octet potential $V_8(r)$

$$\langle \frac{1}{\sqrt{3}} \bar{b}b | \frac{1}{\sqrt{3}} \bar{b}b \rangle \rightarrow V_0(r) = -\frac{4}{3} \frac{\alpha_s}{r} + \mathcal{O}\left(\frac{\alpha_s^2}{r}\right), \quad (\text{S4})$$

$$\langle \frac{1}{\sqrt{2}} \bar{b}\lambda_A b | \frac{1}{\sqrt{2}} \bar{b}\lambda_A b \rangle \rightarrow V_8(r) = \frac{1}{6} \frac{\alpha_s}{r} + \mathcal{O}\left(\frac{\alpha_s^2}{r}\right), \quad A = 1, \dots, 8,$$

while $\langle \frac{1}{\sqrt{3}}\bar{q}q | \frac{1}{\sqrt{3}}\bar{q}q \rangle \rightarrow 1$ and $\langle \frac{1}{\sqrt{2}}\bar{q}\lambda_A q | \frac{1}{\sqrt{2}}\bar{q}\lambda_A q \rangle \rightarrow 1$ are properly normalized to one. The resulting $B\bar{B}^*$ potential at very small r is therefore

$$\begin{aligned} V_{1/r}(r) &= \frac{1}{9}[V_0(r) + 8V_8(r)], \quad V_{1/r}^{O(\alpha_s)}(r) = 0, \\ V_{1/r}(r) &= \frac{1}{9} \frac{4}{3} \frac{\alpha_s}{r} \left(\frac{\alpha_s}{4\pi} \right)^2 \delta a_2. \end{aligned} \quad (S5)$$

The singlet and octet contributions cancel in the case of one-gluon exchange, i.e at the order $O(\alpha_s)$. The lowest non-zero contribution can be obtained from the perturbative calculation of both potentials in [31] and comes at $O(\alpha_s^3)$ with $\delta a_2 = -189.2$. Employing the value of $\alpha_s \simeq 0.31$ obtained from the fit of the singlet $\bar{b}b$ static potential in our simulation, we arrive at $V_{1/r}(r) \simeq -0.0051/r$.

S5: MASS OF THE BOUND STATE FOR VARIOUS FITS

The mass of the bound state depends on the choices of the fit for the potential. The mass in Fig. 4 of the main article was based on the fits of the lattice potential in the ranges $r/a = [2, 4]$, $r/a = [1, 4]$ and form of potential $V(r) = V_{reg.}(r) + V_{1/r}(r)$ in Eq. (5). These masses are shown again in Fig. S3(a,b) for completeness. Two fitting ranges were employed since the lattice potential at $r/a = 1$ can be prone to the lattice discretization errors.

The part of the potential $V_{1/r}(r)$ that is singular as $r \rightarrow 0$ was determined perturbatively (S5) for very small separations r . It is equal to zero at the one-gluon exchange level and the lowest non-zero contribution comes at the order $O(\alpha_s^3)$. The sensitivity of the results on including or excluding this part of the potential is explored in Fig. S3. The masses based solely on the regular potential $V_{reg.}$ in Figs. S3(c,d) agree within errors with masses based on $V_{reg.} + V_{1/r}$ in Figs. S3(a,b). This agreement is a consequence of the suppression in $V_{1/r}$.

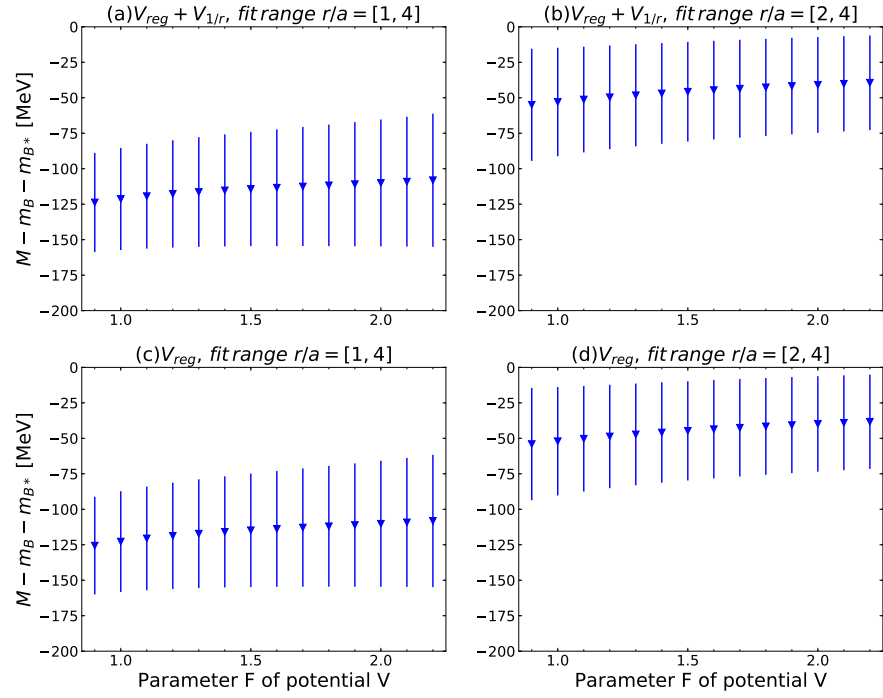


FIG. S3: Mass of the virtual bound state for various choices of the parameter F in $V(r)$ (5). The plot compares results based on the fit of the lattice potentials in the ranges $r/a = [1, 4]$ (left) and $r/a = [2, 4]$ (right). The results based on the potential $V_{reg.} + V_{1/r}$ (top) and $V_{reg.}$ (bottom) are also compared.